Heliyon 6 (2020) e03242

Contents lists available at ScienceDirect

Heliyon

journal homepage: www.cell.com/heliyon

Research article

Design of a radio-frequency transceiver coil for landmine detection in Colombia by nuclear quadrupole resonance

Lorena Cardona [a,b,*], Hideo Itozaki [c], Jovani Jiménez [b], Nelson Vanegas [d], Hideo Sato-Akaba [c]

[a] Department of Mechanical Engineering, Faculty of Engineering, Institución Universitaria Pascual Bravo, Calle 73 No. 73A – 226, Colombia
[b] Department of Computation and Decision Science, School of Mines, Universidad Nacional de Colombia, Carrera 80 No. 65-223, Medellin, Antioquia, Colombia
[c] Department of Systems Innovation, Graduate School of Engineering Science, Osaka University, Toyonaka, Osaka 560-8531, Japan
[d] Department of Mechanical Engineering, School of Mines, Universidad Nacional de Colombia, Carrera 64 No. 63–120, Medellin, Antioquia, Colombia

ARTICLE INFO

Keywords:
Electromagnetism
Nuclear physics
Nuclear quadrupole resonance
Land mines – detection
Explosives – detection
Transceiver coil

ABSTRACT

This paper shows the design of a radio-frequency transceiver coil for landmine detection in Colombia by nuclear quadrupole resonance (NQR). The radio-frequency transceiver coil is of great importance as it is responsible for exciting the target explosive and for picking up the weak NQR signal; however, little detail is found on the literature about its design. The strategy followed on this work consisted on constructing and experimentally comparing five different radio-frequency transceiver coils, whose dimensions were selected according to four design parameters: noise rejection, magnetic flux density, coil sensitivity, and quality factor; taking into account the characteristics of landmines in Colombia, the second country most affected by anti-personnel mines in the world. The constructed coils were experimentally compared using a portable system and with three of them, the system was capable of detecting 200 g ammonium nitrate (the main substance used in Colombian landmines) up to 3 cm from the coil within 12 s, with a steady-state free precession pulse sequence. Conclusions from this work could help to guide RF coil design in other works that apply NQR for remote detection of substances in non-shielded environments and to direct future research about landmine detection in Colombia.

1. Introduction

Nuclear quadrupole resonance (NQR) is a spectroscopic technique, which exploits the fact that nuclei with spin quantum number I greater than ½ have electric quadrupole moment. Interaction of this moment with the surrounding electric field gradient at the nuclei causes splitting of nuclear energy levels. Quadrupolar nuclei can be excited to higher energy levels by applying radio frequency (RF) pulses; after excited, nuclei return to ground state relieving weak RF energy that could be detected. The excitation frequency and the spectrum recorded from each substance is unique, thus NQR can be employed for highly specific detection of substances. One promising application of NQR is landmine detection, since most explosives inside landmines contain ^{14}N, an isotope with spin equal to 1 [1].

Design of the RF coil strongly affects the range and sensitivity of the NQR system as the coil is responsible for sending RF pulses at the specific target frequency for efficient excitation of the substance, and for picking up the weak NQR signal by Faraday's law of induction, usually in a noisy environment. However, in most publications about landmine detection by NQR [1, 2, 3, 4, 5], little attention has been paid to NQR coil design. An exception is the work of Farantatos et al [6], who made an electromagnetic design of a spiral coil in COMSOL Multiphysics for landmine detection; however, they did not considered noise as an important parameter in the design. Other works that deal with NQR coil design, not directly related to landmine detection, include: [7], which compares two-spiral flat coils having uniform and logarithmic windings for detecting NQR signals; and [8], which proposes a simulation method to estimate the detection efficiency of NQR. However, the specific characteristics of the target to be detected, like the size and shape of the enclosure and its depth, were not considered on these works. By incorporating target information in the design process, NQR system performance can be improved, as coil can be optimized for the specific application.

The aim of this work was to design a NQR transceiver coil for landmine detection, taking into account characteristics of landmines in Colombia, a country that ranks second in the world by the number of victims from landmines [9]. As there is no simple function that can be maximized to give the 'best' coil design, we proposed a strategy of

* Corresponding author.
E-mail address: lorena.cardona@pascualbravo.edu.co (L. Cardona).

https://doi.org/10.1016/j.heliyon.2020.e03242
Received 26 February 2019; Received in revised form 29 November 2019; Accepted 14 January 2020

combining theory-guided design with experimental comparison of some constructed coils. First, we incorporated specific information of the targets, such us their diameter, length and expected depth for designing the transceiver coil and then, we constructed five different coils and evaluated their performance in terms of transmitted RF magnetic field, sensitivity for picking up the NQR signal and environmental noise suppression, as these are main factors influencing landmine detection performance.

This work is relevant since the government of Colombia recently signed a peace agreement with the armed group responsible for placing most of the mines on its territory, then Colombia has started humanitarian mine action operations. In addition, the methodology proposed in this study could help to guide RF coil design in future research that applies NQR for remote detection of substances in non-shielded environments.

This paper is organized as follows: section 2 shows the characteristics of landmines in Colombia; section 3 explains each of the criteria taken into account for the design of the transceiver coil; section 4 presents the coils built according to these criteria, as well as the methods for their experimental comparison; section 5 presents the results and their discussion; and section 6 presents the conclusions.

2. Landmines in Colombia and previous work

2.1. Landmines in Colombia

In Colombia, most landmines are made from PVC tubes or common household items such as jars of coffee or bottles of soda, with about 250 g of explosive. Those landmines are made without any metallic parts and are buried at depths between 1 and 8 cm, as shown in Figure 1. Landmine depth depends on its enclosure, as some recipients have longer "bottleneck". Figure 1 shows that the diameter of a typical landmine ranges from 6 to 10 cm, and its length varies between 4 and 16 cm.

2.2. Ammonium nitrate

Ammonium nitrate is in most explosive mixtures inside Colombian landmines [10]. An ammonium nitrate crystal consists of ammonium and nitrate ions linked by N–H–O bonds. When detecting ammonium nitrate by NQR, the ν_- frequency of the ^{14}N nuclei in nitrate ion is usually the target because it is higher than those of ammonium ion and its temperature coefficient is much lower than that of the ν_+ line for the same ion.

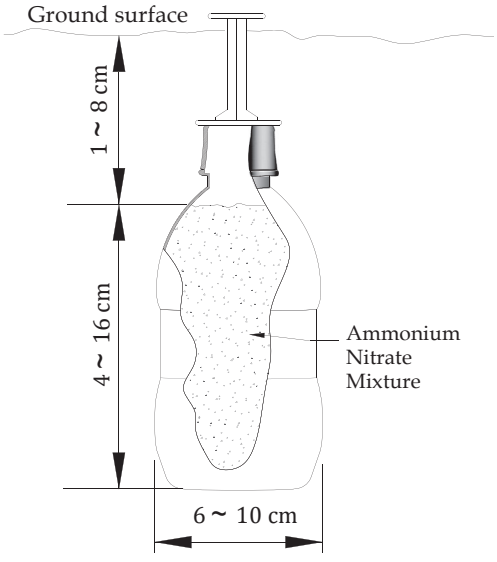

Figure 1. Characteristics of a common Colombian landmine.

ν_- frequency is 423.5 kHz at 25 °C and its temperature coefficient is $+91 Hz/K$. Other properties of this line are: $T_1 = 16$ s and $T_2 = 6$ ms [11].

3. Design criteria

3.1. Noise rejection

Since regular NQR coils normally respond to the presence of any magnetic field, interfering sources like electrical equipment, power lines and radio stations, may generate a response on the system that masks the NQR signal from the target substance. So far, the most effective method for rejecting radio frequency interference (RFI) is shielding; but for landmine detection, shielding is not feasible as targets cannot be enclosed. Instead, when it comes to remote sensing, using a gradiometer coil seems to be the best option for filtering RFI. A first order gradiometer (that measures an approximation to the first spatial derivative of the magnetic field) has two sets of turns, as shown in Figure 2-a and 2-b, and it only captures the magnetic field gradient between these two sets. The currents in these two sets of turns flow in opposite direction with each other, thus, a uniform magnetic field (far field RFI) induces equal currents in the two sets that cancel out. On the other hand, the currents induced by targets near the gradiometer are different in the two sets, and the current gradient is picked up. The second order gradiometer (Figure 2-c) measures an approximation to the second spatial derivative of the magnetic field. Higher order gradiometer configurations are also possible. Gradiometers have the disadvantage of reducing the SNR because the second coil adds thermal noise to the NQR signal (due to its resistance) [12], however, it is a more simple way to reduce noise when compared to the alternative of having ancillary antennas or coils for active RFI cancellation; besides, ancillary antennas do not achieve the desired RFI rejection when the interferences do not correlate.

For landmine detection by NQR, a planar first order gradiometer (like the one in Figure 2-a) is more suitable for the following reasons:

- Axial gradiometers, as the one in Figure 2-b, occupy larger volumes and this is not a desirable property when designing a manual operated system [13].
- The higher the order of the gradiometer the lower its sensitivity. Since the signal to measure is very weak, second or higher order gradiometers are less suited.
- In the planar geometry, both sides of the gradiometer have sensitivity for signal detection and the soil can be interrogated faster.

Size, shape and distance between the two halves (baseline) of the gradiometer are the main parameters to be considered on its design (and

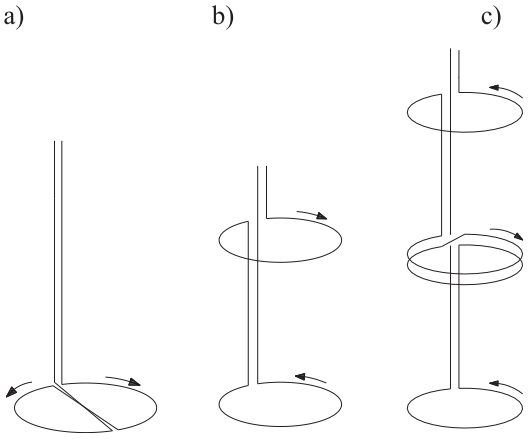

Figure 2. Gradiometer configurations: a) a first order planar gradiometer, b) a first order axial gradiometer, b) second order axial gradiometer.

these are considered on subsequent sections). From the noise rejection point of view, the main aspects are balance and baseline. For the gradiometer shown in Figure 2-a, balance is achieved when left and right sides of the coil are equal. *Baseline* (*b*) is the distance between the two symmetric coils making the gradiometer, and from [14], when *b* increases, noise immunity of the gradiometer decreases while the gradiometer sensitivity gets higher. As these criteria is conflicting and no specific information is known about the noise filtering capacity required for landmine detection in Colombia, baseline was selected according to coil sensitivity criteria, and gradiometer coils with varying baseline were constructed for comparison.

3.2. Transmitted RF magnetic field

The magnetic flux density generated by the coil should be high enough to excite the ^{14}N nuclei, but most important, it should reach the landmine depth. Looking at the circular loop like the one in Figure 3, the magnetic flux density at point P produced by a current i in the loop is given by Eq. (1).

$$B = \frac{\mu_0 i a^2}{2\left(a^2 + h^2\right)^{3/2}} \tag{1}$$

Where $\mu_0 = 4\pi \times 10^{-7}\ H/m$ is the magnetic permeability of free space, a is the radius of the circular loop and h is the distance of point P to the loop. It is assumed that point P lies on the axis of the loop.

A plot of Magnetic flux density vs distance was made from Eq. (1), for different values of a and assuming a constant current of 1A (see Figure 4). The plot shows that the magnetic field generated by smaller loops decay faster with distance than that from larger loops. Depending on the target distance, one particular loop size would be better. Although only the magnetic field at the axis of the loop is being considered, the magnetic flux density at other points are proportional to the field at the axis. Figure 4 only shows plots for coils up to 15 cm radius because larger coils gave very similar results to that of 15 cm.

From Figure 4, magnetic flux density at distances from 3 cm (3 cm is the distance from soil surface to the center of AN filling of the shortest shallowest mine, according to Figure 1) to 16 cm (idem, for the longest deepest mine), are very varied, not being possible to select a single coil with superior performance in the whole range. At a distance of about 9.5 cm (mean depth) coil sizes between 9 cm and 15 cm radius perform very similar and better than the smaller ones. For these coil sizes, the magnetic flux density has more uniform magnitude at the considered target depths. This is a desirable feature since when detecting landmines it is not possible to know beforehand the depth of the target and the RF pulse width that gives the higher SNR depends on magnetic flux density at the nuclei; thus, coils should be designed to project a field of uniform magnitude over the region being investigated [15], making it possible to optimize a single pulse width for the whole depth range.

Thus, from the transmitted RF Magnetic field criteria, coil diameter must be between 18 and 30 cm.

3.3. Sensitivity

One major concern when developing a NQR inductor is its sensitivity. Ideally, a coil should be capable of detecting small quantities of explosive

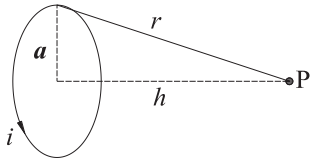

Figure 3. Magnetic flux density at point P, at a distance h from a current carrying circular loop of radius a.

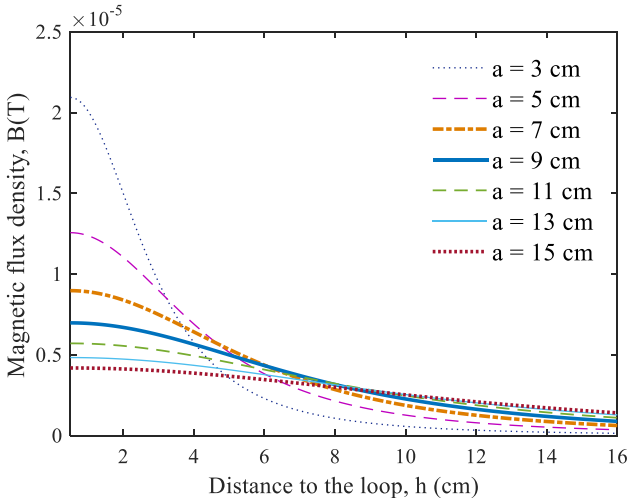

Figure 4. Magnetic flux density vs distance from current carrying loops of different radius. Plot made in Matlab.

at great distances. NQR signal is detected by means of the Faraday's law of induction: NQR signal has a magnetic component oscillating at the resonance frequency, which induces a voltage (or electromotive force *emf*) in the pickup coil. In [1], NQR detection is modeled as a mutual inductance between the sample and the NQR probe, where the observed voltage signal (V_s) is given by Eq. (2). In Eq. (2), Q is the quality factor of the tuned circuit, i is the current in the loop that models the sample, M is the mutual inductance between the sample and the pick-up coil, and ω is the signal frequency.

$$V_s = \omega M i \sqrt{Q} \tag{2}$$

The mutual inductance between two circular coaxial loops of radius a and b, separated by a distance D, is given by Eq. (3) [16], where μ is the magnetic permeability of the medium, and $K(k)$ and $E(k)$ are complete elliptic integrals of the first and second kind, respectively.

$$M = \mu\sqrt{ab}\left[\left(\frac{2}{k} - k\right)K\left(k^2\right) - \frac{2}{k}E\left(k^2\right)\right]$$
$$k = \sqrt{\frac{4ab}{D^2 + (a+b)^2}} \tag{3}$$

Because of the elliptical integral, Eq. (3) has no analytical solution, therefore the relative mutual inductance between the NQR pick-up coil and the sample was calculated for various coil diameters and distances D (see Figure 5), for a 8 cm diameter sample (average target diameter, according to Figure 1). From Figure 5 when the coil and target sizes are similar (higher filling factor), M is larger but only for small distances (about a quarter of the target diameter), as M rapidly decreases with distance. For a depth of about 9.5 cm (mean expected depth), coil diameters between 18 and 30 cm are the best.

Another important consideration in sensitivity is the gradiometer *baseline (b)*. From [14], the sensitivity of the gradiometer starts to decrease for signals coming from distances lower than b. According to this, b should be close to or greater than the expected target depth.

Thus, attending coil sensitivity, coil diameters between 18 and 30 cm are better. This range is consistent with that obtained to maximize magnetic flux density. In addition, to detect samples at 9.5 cm depth, coil baseline should be about 9.5 cm or greater.

3.4. Quality factor

The quality factor, also known as the Q factor, is a dimensionless parameter related to energy losses within a resonant element, relative to

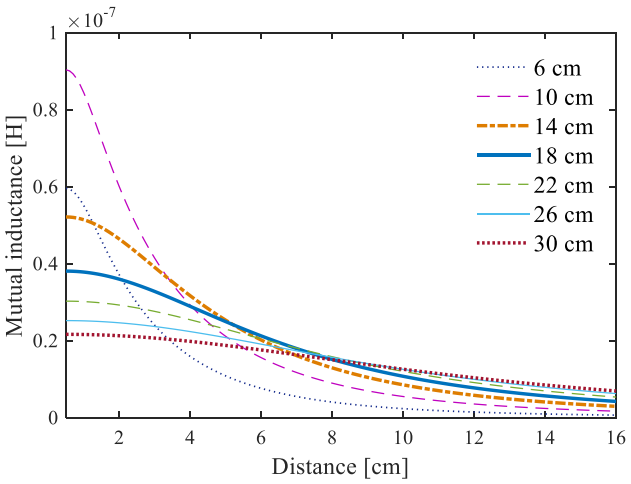

Figure 5. Mutual inductance for the sample and the NQR probe at different distances. An 8-cm diameter is considered for NQR target as well as five coil diameters. This figure was made in Matlab.

the amount of energy stored within the system. Thus, the higher the Q factor the lower the rate of energy loss and hence oscillations will reduce more slowly. The effect of the Q factor can also be appreciated in the frequency domain, as the response of a system with a high Q factor is more narrowly peaked around the resonance frequency, being very sensitive at that frequency, and having very low response at others. On the contrary, an inductor with a low Q factor resonates over a wider range of frequencies.

For landmine detection, a high Q factor is desirable since the inductor will show high sensitivity to the target frequency. However, there is a limit: if the resonance frequency of the inductor does not match that of the target substance, using a coil with a super high Q factor (the one for which the probe bandwidth is close to or narrower than the excitation bandwidth [17]) could result in a very poor system sensitivity due to the narrower bandwidth of the super high-Q coil. Guarantying perfect resonance match in landmine detection is very difficult for two main reasons: first, the frequency of the substance changes with temperature and it is not feasible to know the exact temperature of an underground target; second, the soil can affect the resonance frequency of the system, depending on soil composition and proximity to the coil. In a manually operated detection system, separation from the soil would be difficult to maintain, and soil properties may vary on different locations. In [18], the dependence of the signal to noise ratio (SNR) of a NQR detection system on the Q factor of the coil was studied. The results showed that for off-resonance detection of about 5 kHz (which could be considered typical in a landmine detection tasks), Q factors from 90 to 300 give the best results. Larger values of Q are not desirable as the bandwidth of the coil may become too narrow to accommodate unknown shifts in NQR frequency associated with unknown temperature or soil effects.

From the results of [18], Q factors from 90 to 300 were the goal on the design. The Q factor of the coil was varied by varying the inductance (and therefore, the size) of the coil. Although the Q factor of a resonant coil depends on the connection of other elements to the coil, the configuration of the circuit elements was not modified.

4. Methods

4.1. NQR portable system

On this work, the portable system for remote detection of ammonium nitrate, developed by Cardona et al [19], was used. This system uses the transceiver circuit design from [20]. It has a transmit–receive switch circuit that uses a bipolar transistor to change the quality factor of the receiver circuit by switching its resistance. The transmit-receive circuit (transceiver unit) is shown in Figure 6. It comprises diodes D_1 (11EQS04), $D_2 - D_5$ (SBYV27-200, Vishay General Semiconductor), and $D_6 - D_{11}$ (1N4148); TRI integrated switches S_1, S_2 (MD0100, Supertex Inc.) and S_3 (MD0105); a bipolar transistor Q_1 (FZT853, Diodes Inc.); resistances R_2 (10 Ω) and R_1 (500 Ω); a capacitor C_1 (1 μF); tuning capacitors C_p, C_s and C_{s2} (C series, high voltage type, TDK Corp); and a resistive feedback transimpedance amplifier (Pre-amp) made of a low noise and high-speed operational amplifier (LT6200, Linear Technology Corp). Complete information about the functioning of this transceiver unit can be found in [20].

4.2. Design of the NQR probe

There is no simple function that can be maximized to get the 'best' gradiometer design; therefore, the approach adopted here was a combination of theory-guided design with experimental comparison.

Figure 7 shows the basic shape of the designed coils. From this shape, four different coils were made, varying their size, baseline and number of

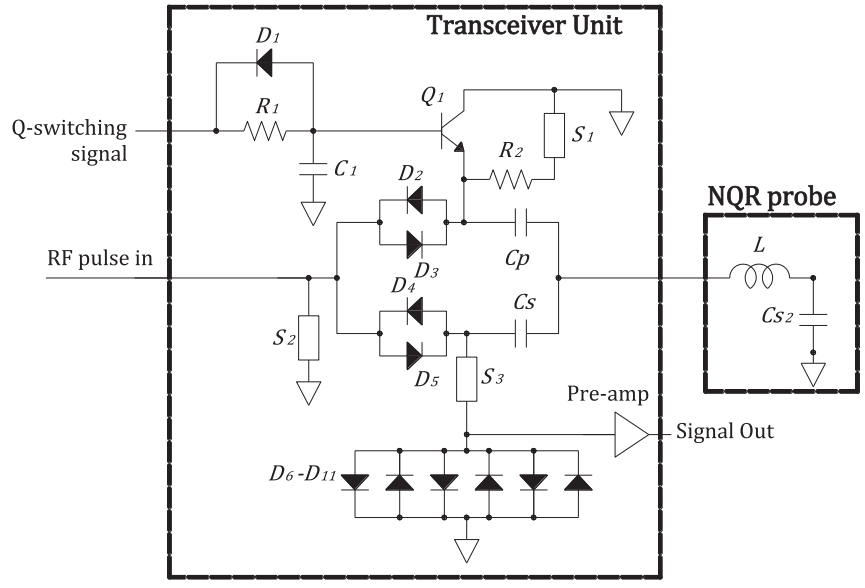

Figure 6. Transceiver unit of the NQR system used on this work, designed by Akaba [20].

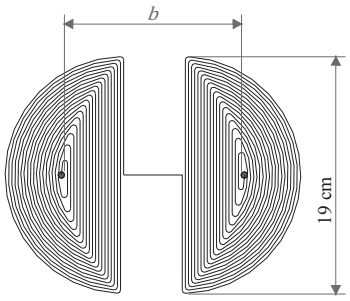

Figure 7. Gradiometer coil design. Black dots are connection ports to capacitors and to the NQR system.

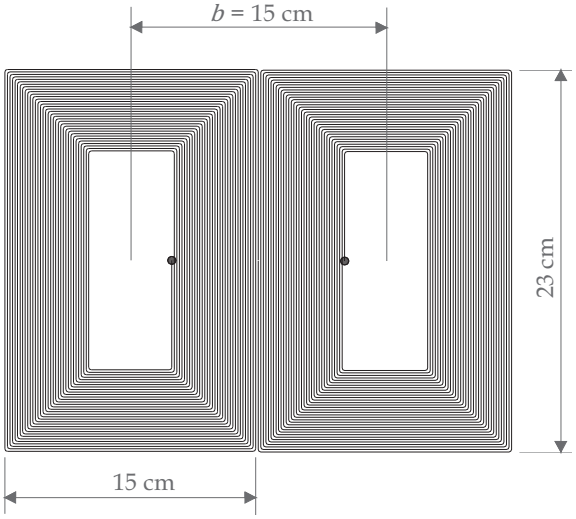

Figure 8. Gradiometer coil E. Black dots are connection ports to capacitors and to the NQR system.

turns. The dimensions of the constructed coils as well as tuning capacitance (C_p, C_s and C_{s2}, according to Figure 6) are presented in Table 1.

The shape on Figure 7 was selected for its compactness, having each half wound in opposite directions to make a gradiometer. The size of coils A, B and C are within the appropriate diameter range to maximize magnetic flux density during excitation, and sensitivity during reception. In addition, the baseline of coil A is of the order of the mean target depth, and baseline of other coils are higher, to see the effect of baseline on sensitivity and noise immunity of the gradiometer. Coils C and D have more turns than coils A and B, for achieving higher inductance and $\boldsymbol{Q}$ factor. Finally, the coil in Figure 8 (coil E) was made with the same number of turns as coil D, and almost the same size, but with different shape.

All the gradiometers were made of copper wire of 0.5 mm in diameter. Each coil shape was drawn in AutoCAD 2014, printed and glued to a wooden table. Then, the copper wire was wound on the table following the printed path, using glue at regular intervals to fix the wire to the table.

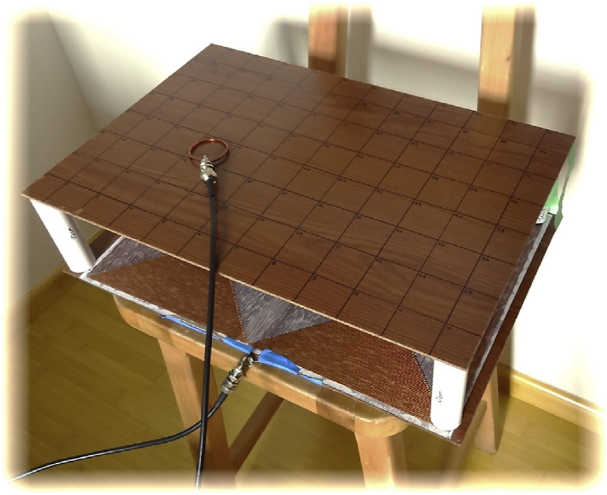

Figure 9. Experimental setup to measure the magnetic flux density generated by each coil at various distances.

4.3. Method for measuring noise

To assess the ability of the inductors to filter noise, each, coil was connected to the NQR equipment and the signal captured by the coil on a ground field was acquired and registered in the absence of ammonium nitrate. This was repeated 50 times, waiting 0.3 s between acquisitions. Acquired time domain data were transformed into the frequency domain by Fast Fourier Transform (FFT), and then averaged. Data were processed in LabVIEW (National Instruments Corp.). Noise spectrum of the system, including the coil, tuning capacitance and the pre-amplifier of the transceiver unit, was obtained from simulation in LTspice IV (Linear Technology Corp.).

4.4. Method for measuring magnetic flux density

Magnetic flux density was measured at various distances from the coil with the experimental setup shown in Figure 9. Each coil was connected to the NQR device and fed with a sinus waveform voltage at the resonance frequency. A board with a drawn grid was located at various distances from the coil and the voltage induced on a circular loop, connected to an oscilloscope, was measured at each of the squares of the grid. The electromotive force (*emf*) induced on the loop by the changing magnetic field is given by Eq. (4).

$$emf = -\frac{d\Phi}{dt} \quad [V] \tag{4}$$

Where Φ is the magnetic flux through the loop, defined by Eq. (5).

$$\boldsymbol{\Phi} = \int_s \mathbf{B} \cdot d\mathbf{s} \tag{5}$$

Where s is the area of the loop and $\mathbf{B}$ is the magnetic flux density. Eq. (5) shows that only the magnetic field component perpendicular to the loop is responsible for the induced electromotive force. Assuming a sinusoidal

Table 1. Parameters of the coils made from the templates in Figures 7 and 8. Capacitance are given according to Figure 6.

coil	number of turns	Inductance (μH)	Resistance (Ω)	b (cm)	C_p (nF)	C_s (nF)	C_{s2} (nF)
A	18.5	58	1	9.5	4.18	0.691	4.87
B	18.5	58	1.1	14	4.15	0.725	4.87
C	24	96.5	1.8	14	2.37	0.56	2.93
D	34	642	5	15	0.3	0.139	0.44
E	34	670	5.5	15	0.28	0.140	0.42

magnetic field generated by the coil $B = B_0 \sin(\omega t)$, the *emf* induced on the loop is given by Eq. (6).

$$emf = -B_0 \omega s \cos(\omega t) \quad = \quad emf_0 \cos(\omega t) \tag{6}$$

Where $emf_0 = -B_0 \omega s$ is the amplitude of the electromotive force induced on the circular loop. Thus, the amplitude of the magnetic flux density could be calculated by measuring the amplitude of the *emf* on the loop by Eq. (7).

$$B_0 = -\frac{emf}{\omega s} \tag{7}$$

This way, a two-dimensional map of the magnetic flux density generated by each coil at various distances was made.

4.5. Method for measuring coil sensitivity

To measure the amplitude of the signal picked up by the coil, the same experimental setup on Figure 9 was employed, but in this case the loop was connected to a signal generator and fed with a 50 mV sinusoidal voltage at the coil resonance frequency (423.5 kHz). The loop was placed at each of the cells of the board with the drawn grid and the amplitude of the signal picked up by the coil was measured. The board was placed at various distances from the coil, and this way, a two-dimensional sensitivity map of the inductor was generated for various distances.

4.6. Method for measuring coil quality factor

The quality factor of each coil was measured from the time response. A pulse at the resonance frequency was fed to the coil through the transceiver unit and the Q factor was computed from the shape of the pulse (corresponding to the voltage measured across the coil) using Eq. (8).

$$Q = \pi f_0 \tau \tag{8}$$

Where f_0 is the resonance frequency in Hz and τ is the decay time, equivalent to the time it takes for the oscillation to decay from A (the start amplitude) to A/e.

The NQR system has a Q switching function to lower the Q factor of the NQR probe during a short time after pulsing, to accelerate coil recovering, so it is ready to pick up the NQR signal faster. Therefore, the probe has two Q factors, a high one when the switching function is on, and a low one when it is off. To measure the high and low Q factors of each coil, a 50 mV sinusoidal voltage at the resonance frequency of the coil was fed into a loop (4 cm in diameter) in burst mode (500 μs on and 500 μs off), using a signal generator (Digilent Analog Discovery). The loop was placed at 9 cm from the coil, and the voltage induced in the coil was captured with an oscilloscope (Digilent Analog Discovery). This was done while the Q-switch was on (high Q) and off (low Q). The Q factor in both cases was computed from Eq. (8).

4.7. Method for detecting ammonium nitrate

The NQR signal from 200 g of ammonium nitrate at various distances from the coil was picked up using a SSFP sequence with the parameters specified in Table 2. Ammonium nitrate was in a plastic bottle like the one shown in Figure 1 that was 6 cm in diameter and 14 cm long. The detection was made on a ground field in Colombia.

Table 2. Parameters of the SSFP sequence.

Pulse width	200 μs
Repetition time	2,2 ms
Number of pulses	3.000
Total time of the sequence	6,6 s

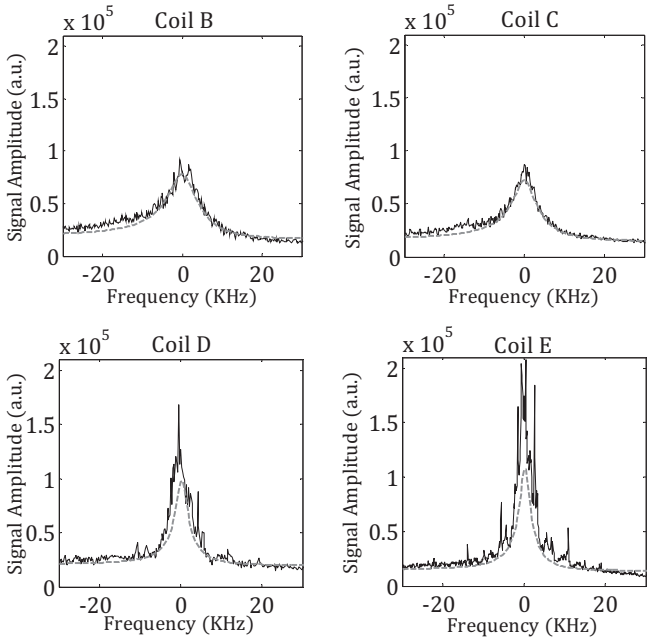

Figure 10. Noise spectra of coils B to E measured in the outdoors (solid line) and simulated on LTspice (dashed line). On the horizontal axis, zero is the reference frequency (423.5 KHz).

5. Results and discussion

5.1. Results and discussion for noise filtering

Noise spectra of the coils are displayed in Figure 10. As coils A and B gave very similar results, only one of them (coil B) is shown.

The broad peaks of the noise spectra in Figure 10 were due to the resonance of the probes that were tuned at the NQR frequency of ammonium nitrate. From Figure 10, the coils with the highest quality factors (coils D and E) were not very good at filtering noise. Although higher noise peaks were expected from these coils due to their larger resistance (see Table 1), which translates into higher thermal noise [15], the experimental results showed that the noise spectra obtained in the outdoors for these coils were higher than expected from simulation, especially for coil E. One factor that could have affected noise filtering was the long baseline, which made the coil more sensitive to near-field sources of noise. However, baselines of coils D and E were only 1 cm longer than that of coils B and C, which showed very good noise filtering capabilities. Hence, noise in coils D and E were most probably caused by a lack of balance (lack of symmetry). To filter noise, a gradiometer coil must be well balanced, and in a hand wound coil, balance is hard to accomplish, even more if the coils are big.

5.2. Results and discussion for magnetic flux density

The two-dimensional map of the magnetic flux density generated by coils A and E at various distances are shown in Figure 11. As the gradiometer has two symmetric sides, only half of the magnetic field map is shown in the figure. In addition, as the results from coils A, B and C were very similar, only one of them is presented. Coil D is also omitted because its figure was very similar to that of coil E. Data of magnetic flux density is presented in the supplementary material (files coilA_magnetic_field and coilE_magnetic_field).

The magnetic flux density generated by the planar gradiometers was higher at the center of each half coil. The largest difference between the gradiometers was at 4 cm, where the magnetic flux density from coils D

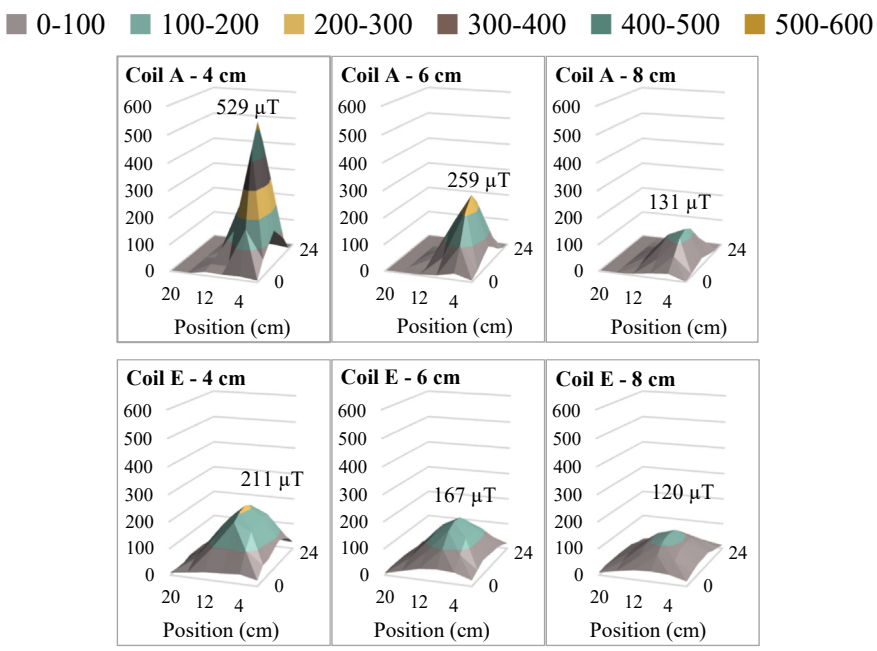

Figure 11. Magnetic flux density generated by coils A and E at various distances. Only the left half of the magnetic field map is displayed. The position (0,0) on the plots corresponds to the bottom center of the grid.

and E where much lower than that generated by coils A to C. At 6 cm, differences in magnetic flux densities were smaller, and at 8 cm they were almost equal. This is consistent with theory (Figure 4); inductors of higher sizes generate magnetic fields of lower amplitudes near the coil, but their amplitudes have lower rates of decay with distance.

5.3. Results for sensitivity

The two-dimensional sensitivity maps of the coils at various distances are presented in Figure 12. As the gradiometers have two symmetric sides, only half of the sensitivity maps are displayed in the figure. Coils A, B and C had very similar results, and results from coils D and E were also very similar to each other; therefore, only the maps of coils A and E are shown in Figure 12. Data of coil sensitivity is presented in the supplementary material (files coilA_sensitivity and coilE_sensitivity).

From Figure 12, the sensitivity of the planar gradiometers was higher at the center of each half-coil. Although coils A and B had different baseline (9.5 cm and 14 cm, respectively), their results were very similar, indicating that the baseline did not have an impact on the sensitivity. Coils D and E had superior sensitivity than the others. Even at 8 cm from the source, their sensitivity was almost the same as that of the other coils at 6 cm, and about 1.5 times higher than the other coils at the same distance. This was not expected from the sizes of these coils, because the mutual inductance between the small loop used for excitation and coils D and E was expected to be low (because of the lower filling factor). Therefore, the high sensitivity of the largest coils should be due to their higher Q factor.

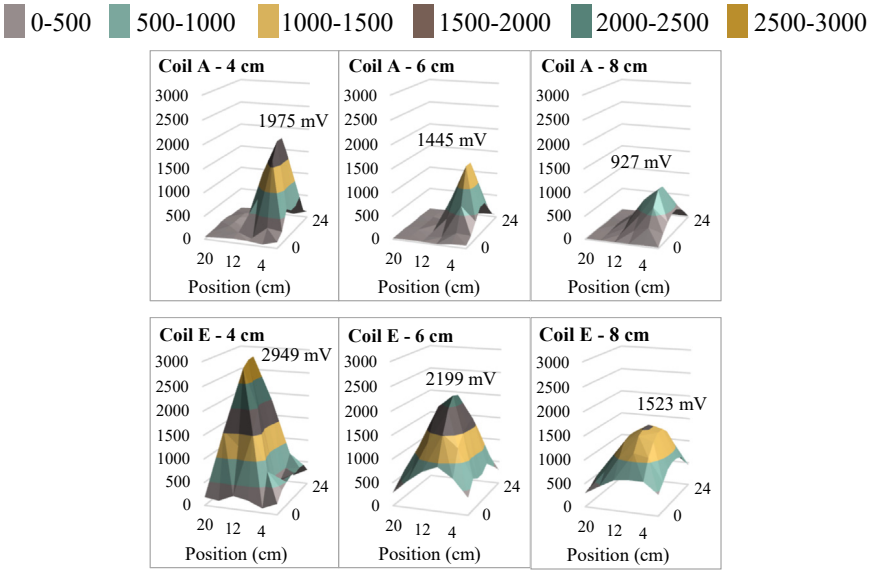

Figure 12. Sensitivity of the coils A and E to a signal generated by a circular loop. Only the left half of the sensitivity map is presented since the inductors are symmetric. The position (0,0) on the plots corresponds to the bottom center of each coil.

Table 3. Low and high *Q* factors for the five inductors.

Inductor	High Q	Low Q
A	70	15
B	69	14
C	78	19
D	119	34*
E	141	47*

* Values taken from part of the plot, as the voltage shape showed two different values of *Q* for coils D and E.

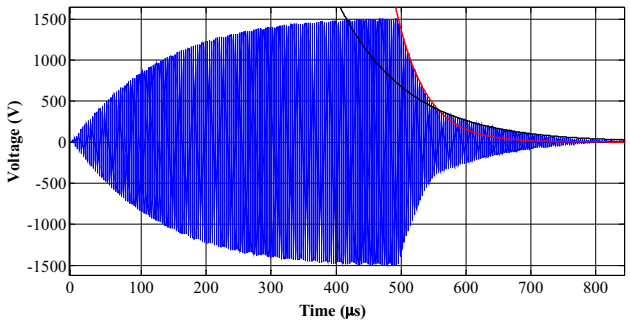

Figure 13. Voltage in coil D when the *Q*-switch was off. The *Q* factor is lowered, but it gets higher again after Voltage on the coil falls down to about 400 V. Two exponential curves can be fitted to represent signal decay.

5.4. Quality factor results

The measured *Q* factors of the five inductors are presented on Table 3.

Although the *Q*-switching system showed high capability for lowering the *Q*-factor of the probes, for coils D and E this was only partly true. As shown in Figure 13 for coil D (the same happened for coil E), while the *Q* switch was off, the *Q* factor was lower (34) but it got higher again (119) when the voltage in the coil dropped to about 400 V. This was due to the design of the *Q* switch in the transmission circuit [20].

5.5. NQR signal from AN

The detection of ammonium nitrate was only made with coils A to C, and as expected, they gave very similar results. The results for coil C are presented in Figure 14 (results for coils A and B are omitted as they were very similar to those of C). Ammonium nitrate was not detected using coils D and E because of their still high *Q*-factor after pulsing, which made impossible to pick up the weak NQR signal. The detection of ammonium nitrate with coils A to C was possible for 200 g of ammonium nitrate to a distance of 3 cm, measured from the coil to the top of the AN filling. Since the length of the enclosure was 14 cm, this was equivalent to a distance of 10 cm from the middle of the filling. This was an improvement from [19], where the same amount of ammonium nitrate was detected in a wider enclosure (10 cm in diameter and 5 cm long), with most of the substance being closer to the coil. In the present case, the enclosure was narrower and longer (as expected in Colombian landmines), with less substance being close the coil.

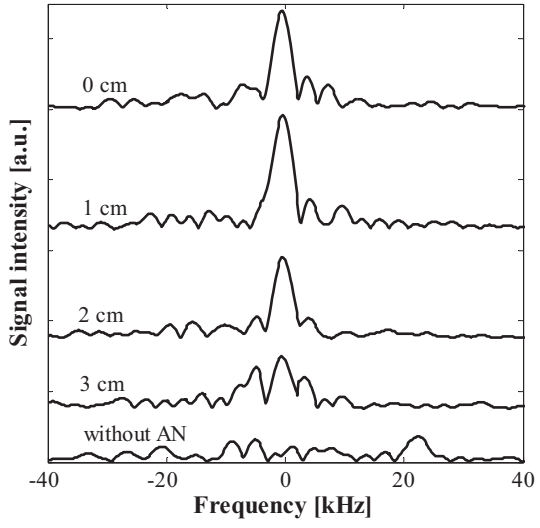

Figure 14. Signal intensity of 200 g of AN at various distances from the coil, with 3.000 pulses of SSFP.

Although the coils were designed for detecting targets at depths from 1 to 8 cm, measured from ground surface to the top of the target, the NQR signal from ammonium nitrate could only be detected down to 3 cm. The reason for this is that NQR signal intensity was not considered on the design. At low frequencies, as that of ammonium nitrate, NQR signal is weak and it would require the repetition of the whole SSFP sequence to accumulate enough number of acquisitions to get a signal high enough to be detected. However, the repetition of the SSFP sequence would require a dead time of more than one minute between the sequences (as T_1 for ammonium nitrate is 16 s at 25 °C), and for landmine detection, that time is very long.

6. Conclusions

The followed methodology for transceiver coil design, which considered the properties of the targets to be detected, lead to a functional coil, capable of detecting 200 g of ammonium nitrate at 3 cm from the coil, in an enclosure that was 6 cm in diameter and 14 cm long, similar to a typical landmine in Colombia. This was achieved with three of the five designed coils, being all planar first order gradiometers of circular shape (each half of the coil having the shape of a half circle).

Although bigger coils were made, having larger *Q*-factors and higher sensitivity, they had poor performance for noise filtering, which was attributed to a lack of balance as these coils had many turns and were wounded by hand. Additionally, the *Q*-switching system of the NQR device used on this work could not lower the *Q*-factors of the biggest coils for long enough after pulsing, which prevented the detection of the weak NQR signal from Ammonium Nitrate. Since for landmine detection sensitivity is of paramount importance, bigger coils having higher sensitivity deserve further research. Their higher *Q*-factors makes them more sensitive and due to their size, the magnitude of the magnetic flux density is more uniform over the considered target depths, making it possible to optimize a single pulse width for the whole depth range as the RF pulse width that gives the higher SNR depends on magnetic flux density at the nuclei.

Future research will focus on trying more precise winding techniques for making the larger coils and on re-designing the *Q*-switching system of the NQR device to get and maintain a lower *Q* factor after pulsing. In addition, optimizing gradiometer design using a software as Comsol Multiphisics, like in the work of Farantatos et al [6], could help to improve de design of the coils before experimental comparison.

Declarations

Author contribution statement

Lorena Cardona: Conceived and designed the experiments; Performed the experiments; Analyzed and interpreted the data; Contributed reagents, materials, analysis tools or data; Wrote the paper.

Hideo Itozaki, Hideo Sato-Akaba: Conceived and designed the experiments; Contributed reagents, materials, analysis tools or data; Wrote the paper.

Jovani Jiménez: Analyzed and interpreted the data; Wrote the paper.

Nelson Vanegas: Analyzed and interpreted the data; Contributed reagents, materials, analysis tools or data; Wrote the paper.

Funding statement

This work was supported by Japan Society for the Promotion of Science and Administrative Department of Science, Technology and Innovation of Colombia (COLCIENCIAS).

Competing interest statement

The authors declare no conflict of interest.

Additional information

Supplementary content related to this article has been published online at https://doi.org/10.1016/j.heliyon.2019.e02697.

References

[1] A.N. Garroway, M.L. Buess, J.B. Miller, B.H. Suits, A.D. Hibbs, G.A. Barrall, R. Matthews, L.J. Burnett, Remote sensing by nuclear quadrupole resonance, IEEE Trans. Geosci. Rem. Sens. 39 (2001) 1108–1118.

[2] A.D. Hibbs, G.A. Barrall, P.V. Czipott, A.J. Drew, D.K. Lathrop, Y.K. Lee, E.E. Magnuson, R. Matthews, D.C. Skvoretz, S.A. Vierkotter, Man portable mine detector using nuclear quadrupole resonance - first year progress and test results, in: Second Int. Conf. Detect, Abandon. L. Mines, Edinburgh , UK, 1998, pp. 138–141.

[3] A.D. Hibbs, In-Situ Real Time Detection of Explosive-Chemical Compounds in Mines Using Nuclear Quadrupole Resonance, NQR), San Diego, CA, 2001. http://www.dtic.mil/cgi-bin/GetTRDoc?AD=ada388897.

[4] M. Ostafin, B. Nogaj, 14N-NQR based device for detection of explosives in landmines, Measurement 40 (2007) 43–54.

[5] H. Itozaki, Nuclear quadrupole resonance for explosive detection, in: K. Furuta, J. Ishikawa (Eds.), Anti-Personnel Landmine Detect. Humanit. Demining Curr. Situat. Futur. Dir. Japanese Res. Dev., Springer - Verlag, London, 2009, pp. 148–155.

[6] P. Farantatos, J. Barras, I. Poplett, P. Kosmas, Electromagnetic design of a spiral surface RF-coil transceiver for NQR-based explosive detection in the humanitarian demining setting, in: Proc. 2018, COMSOL Conf., Lausanne, 2018.

[7] G.V. Mozzhukhin, A.V. Efremov, A.V. Bodnya, V.V. Fedotov, A two-spiral flat coil for detecting 14 n nqr signals, Russ. Phys. J. 48 (2005) 978–983.

[8] J. Shinohara, H. Sato-Akaba, H. Itozaki, Simulation of nuclear quadrupole resonance for sensor probe optimization, Solid State Nucl. Magn. Reson. 43–44 (2012) 22–26.

[9] L. Cardona, J. Jiménez, N. Vanegas, Nuclear quadrupole resonance for explosive detection, Ingeniare 23 (2015) 458–472.

[10] Y.A. Pino, Determinación de técnicas de detección de explosivos óptimas para el departamento de antioquia, Universidad Nacional de Colombia, sede Medellín, 2009.

[11] J. Barras, M.J. Gaskell, N. Hunt, R.I. Jenkinson, K.R. Mann, D.A.G. Pedder, G.N. Shilstone, J.A.S. Smith, Detection of ammonium nitrate inside vehicles by nuclear quadrupole resonance, Appl. Magn. Reson. 25 (2004) 411–437.

[12] H. Robert, E.E. Magnuson, Nuclear Quadrupole Resonance System and Method of Using the Same to Remove Interference Components from Sensor Signals, US9575147B2, 2017. https://patents.google.com/patent/US9575147.

[13] K.D. Singh, The Development of Biomagnetic Systems: Planar Gradiometers and Software Tools, The Open University, 1991.

[14] B.H. Suits, The noise immunity of gradiometer coils for 14N N Q R land mine Detection: practical limitations, Appl. Magn. Reson. 25 (2004) 371–382.

[15] M.L. Collins, Detecting Body Cavity Bombs with Nuclear Quadrupole Resonance, Northeastern University, 2014. https://pdfs.semanticscholar.org/6c04/5c3813f8d4bc8cff7030f4d142d9eaa9c427.pdf?_ga=2.106766083.1290705002.1573739873-1792956156.1573739873.

[16] S.F. Pichorim, P.J. Abatti, Design of circular and solenoid coils for maximum mutual inductance, in: T. Penzel, S. Salmons, M.R. Neuman (Eds.), Biotelemetry XIV Proc. Fourteenth Int. Symp. Biotelemetry, Tectum Verlag, Marburg, Germany, 1997, pp. 71–76.

[17] B.H. Suits, A.N. Garroway, J.B. Miller, Super-Q detection of transient magnetic resonance signals, J. Magn. Reson. 132 (1998) 54–64.

[18] A. Gregorovič, T. Apih, Aplicability of TNT "super-Q detection" to multipulse sequences, J. Magn. Reson. 201 (2009) 131–136.

[19] L. Cardona, Y. Miyato, H. Itozaki, J. Jimenez, N. Vanegas, H. Sato-Akaba, Remote detection of ammonium nitrate by nuclear quadrupole resonance using a portable system, Appl. Magn. Reson. 46 (2015) 295–307.

[20] H. Sato-Akaba, Design and testing of a low impedance transceiver circuit for nitrogen-14 nuclear quadrupole resonance, Solid State Nucl. Magn. Reson. 63–64 (2014) 30–36.